Effect of Convex Wall Curvature on Three-Dimensional Behavior of Film Cooling Jet

Sang Woo Lee
School of Mechanical Engineering, Kumoh National University of Technology, Kumi, Kyongbuk 730-701, Korea
Joon Sik Lee*, Keon Kuk
School of Mechanical & Aerospace Engineering, Seoul National University, Seoul 151-742, Korea

The flow characteristics of film coolant issuing into turbulent boundary layer developing on a convex surface have been investigated by means of flow visualization and three-dimensional velocity measurement. The Schlieren optical system with a spark light source was adopted to visualize the jet trajectory injected at 35° and 90° inclination angles. A five-hole directional pressure probe was used to measure three-dimensional mean velocity components at the injection angle of 35°. Flow visualization shows that at the 90° injection, the jet flow is greatly changed near the jet exit due to strong interaction with the crossflow. On the other hand, the balance between radial pressure gradient and centrifugal force plays an important role to govern the jet flow at the 35° injection. The velocity measurement shows that at a velocity ratio of 0.5, the curvature stabilizes downstream flow, which results in weakening of the bound vortex structure. However, the injectant flow is separated from the convex wall gradually, and the bound vortex maintains its structure far downstream at a velocity ratio of 1.98 with two pairs of counter rotating vortices.

Key Words: Film Cooling Jet, Convex Wall, Velocity Ratio, Injection Angle, Flow Visualization, Three-Dimensional Velocity Measurement

Nomenclature

D : Inner diameter of the injection pipe
J : Momentum flux ratio, $J=\rho_j U_j^2/\rho_\infty U_{pw}^2$
P_r : Total pressure outside the boundary layer
P_{sw} : Static pressure at the wall
P_t : Total pressure
R : Velocity ratio, $R=U_j/U_{pw}$
r_w : Radius of curved wall
Re_D : Injection pipe flow Reynolds number, $\mathrm{Re}_D=U_jD/\nu$
Re_{pw} : Crossflow Reynolds number, $\mathrm{Re}_{pw}=U_{pw}D/\nu$
U, V, W : x, y and z-components of mean velocity
U_e : Mean velocity at the jet exit without crossflow
U_j : Mean velocity averaged across the jet exit, $U_j=\frac{4}{\pi D^2}\int_0^{D/2} U_e 2\pi r dr$
U_p : Potential velocity in the x-direction
U_{pw} : Potential velocity at curved wall in the x-direction
x, y, z : Coordinates in the streamwise, radial and spanwise directions
α : Inclination angle of the injection pipe
δ : Boundary layer thickness
δ^* : Displacement thickness, $\delta^* \equiv \int_0^\infty \left(1-\frac{U}{U_p}\right)dy$
θ : Momentum thickness, $\theta \equiv \int_0^\infty \frac{U}{U_p}\left(1-\frac{U}{U_p}\right)dy$

* Corresponding Author,
E-mail : jslee@gong.snu.ac.kr
TEL : +82-2-880-7117; **FAX** : +82-2-880-0179
School of Mechanical & Aerospace Engineering, Seoul National University, Seoul 151-742, Korea. (Manuscript **Received** July 3, 2001; **Revised** May 17, 2002)

ν : Kinematic viscosity
ρ_j : Injectant density
ρ_∞ : Crossflow fluid density
Φ_j : Mean vorticity flux
Ω_j : Spatially averaged mean vorticity over cross-section of the injection pipe
Ω_x : Streamwise mean vorticity

1. Introduction

In modern aircraft gas turbine engines, the turbine inlet temperature has steadily been increased to meet high engine performance. Of recently developed gas turbines, turbine blades operate in extremely high temperature environment well above the allowable material limit even for ceramics. Film cooling is one of the most widely applied cooling methods, in which the turbine blade is protected by injected coolant from being overheated. For development of improved film cooling, it is essential to understand the flow behavior which exerts an important effect on heat transfer during film cooling process. Turbine blade surfaces usually have curvatures which seem to alter the flow field significantly on the film-cooled surfaces. However, there are few reports which investigate the effect of curvatures on three dimensional jet flow injected into the turbulent boundary layer over a convex surface.

In an inviscid, irrotational flow over a convex surface, velocity decreases as moving away from the center of curvature in the radial direction. If a fluid element traveling in a circular path in equilibrium is displaced a small distance away from the center of curvature, a simple force balance analysis on this element shows that the radial pressure gradient at its new location is slightly larger than what is necessary to move it in a new circular path. The element is then forced back towards the original streamline. Conversely, if an element is displaced towards the center of curvature, the pressure gradient at its new location is not strong enough to bend its path around the tighter radius of curvature and it will move back out towards its original equilibrium position. In an inviscid, irrotational flow with convex curvature, then, there is a natural tendency for a fluid element to stay close to the particular streamline where their velocity is matched to the local radial pressure gradient. For a turbulent flow over a convex wall, if a fluid element moves outward across mean streamline into regions of higher mean velocity, its mean centrifugal force will be less than the new mean radial pressure gradient, resulting in a net restoring force. Therefore, convex boundary layer should exert a stabilizing influence on turbulent momentum exchange.

The inclusion of a jet into the crossflow boundary layer can alter the flow field substantially and results in a very complex three-dimensional flow structure. Many investigations have been made into this type of flow since Morton (1961), and Keffer and Baines (1963) in the case of no surface curvature. Kamotani and Greber (1972) measured the average velocity, turbulent components, and the temperature distributions for normally injected round jet in a crossflow. They found that the measured quantities were dependent mainly on the momentum flux ratio of the jet to the crossflow and revealed the existence of a pair of counter-rotating vortices. Moussa et al. (1977) found from three-dimensional velocity measurements that a pair of bound vortices were formed in the downstream region due to the reorientation of ring vortex, emerging from the pipe, by interaction with the crossflow. Andreopoulos and Rodi (1984) studied experimentally for the injected round jet in the presence of boundary layer flow on a flat wall, and showed that the jet structure was dependent strongly upon the velocity ratio. They also suggested two kinds of flow patterns according to the velocity ratios. Using a conditional sampling technique, Andreopoulos(1985) clarified that irrotational crossflow did contribute to the average turbulent quantities, while the jet-pipe irrotational flow did significantly to them. The above studies were mainly for the normally injected jet in a crossflow over a flat wall.

Lee et al. (1994) studied three-dimensional flow structure of a streamwise inclined jet injected into turbulent boundary layer developing over a flat wall. Their flow visualization showed that the normally injected jet lost its pipe-flow character

just downstream of the jet exit and resulted in a highly turbulent and intermittent flow situation. On the other hand, flow of the streamwise inclined jet with 35° showed very different behavior from that of the normally injected jet. The inclined jet maintained its structure far downstream with relatively small interactions with crossflow. Furthermore, they showed a well organized three-dimensional spiral flow without reverse flow.

Ko et al. (1984) studied a jet with 30° inclination issuing into the boundary layer over a convex wall of a curved duct. They measured mean and turbulent velocities only in a jet symmetry plane with a LDA, although they focused mainly on the measurement of the film-cooling effectiveness. In their result, the effect of strong streamwise pressure gradient might be included in addition to the curvature effect, because the injection hole was situated at the inlet plate of a convex wall.

In this study, three-dimensional velocity measurements have been carried out to investigate the effect of the convex curvature on a round jet injected at 35° inclination into a turbulent boundary layer over a convex wall. In addition, the behavior of the inclined jet is compared with that of a normally injected jet through flow visualizations.

2. Experimental Apparatus and Procedure

The wind tunnel used was an open-circuit type. At a mean velocity of 10 m/s, the uniformity and turbulent level were about 0.5% and 0.2%, respectively. As shown in Fig. 1, the experimental set-up comprises of three regions: an entrance region where the flow from the wind tunnel is developing to a turbulent boundary flow ; a curved region with a 90° bend ; and an exit region where the flow passed over the curved surface is recovering. The entrance and exit regions were made of rectangular ducts of 0.4 m in width and 0.12 m in height and the lengths of inlet and outlet were 0.8 m and 0.6 m, respectively. The flow emerging from the wind tunnel was developing to the turbulent boundary layer flow right after the trip wire of 0.5 mm in radius. The curved surface was made of PVC, 12 mm in thickness, and the radius of the curvature was 0.25 m. The jet exit was located at 80 mm from the beginning of the curved region with 35° inclination. The injection pipe had inner diameter of 24 mm and length of 1.2 m. Before entering the injection pipe, the injected air from the blower passed through a heat exchanger and a plenum chamber. The temperature difference between the boundary layer flow and jet was controlled to within 0.5℃. In general, when the boundary layer flow entered from a flat plate to a convex surface, the static pressure decreased on the convex surface. Hence on the convex surface, favorable pressure gradient always existed in the streamwise direction. Since the main purpose of the present study was to investigate solely the effect of the convex curvature, the opposite wall of the curved region was adjusted to minimize the effect of the streamwise pressure gradient. The adjustment was made by modifying the shape of two wood frames to which the opposite wall made of compressed paper board with thickness of about 2 mm was fastened. After many times of trial and error, the final shape of the wall was determined as shown in Fig. 1.

The measurement system employed in this study was nearly the same as that of Lee et al. (1994). For the visualization study, a Schlieren optical system (Ito Koken Co.) was employed with a spark-light source to obtain instantaneous photographs. The side walls of the curved region were replaced by two optical quality windows, and CO_2 gas with 99.9% purity was delivered from a high pressure container to the injection pipe via a pressure regulator, a calibrated flow meter and a plenum. A five-hole three-dimensional directional probe with tip diameter of 3.1 mm (United Sensor & Control DC125) was used for measurements of three-dimensional velocity components. Three-dimensional velocity components were determined from the calibration curves obtained from the relations among pressures at five holes, yaw and pitch angles, and velocity magnitudes. In order to locate the probe, a special traverse mechanism with a precise rotational accuracy was applied to the movement in the x-direction, on which two stepping

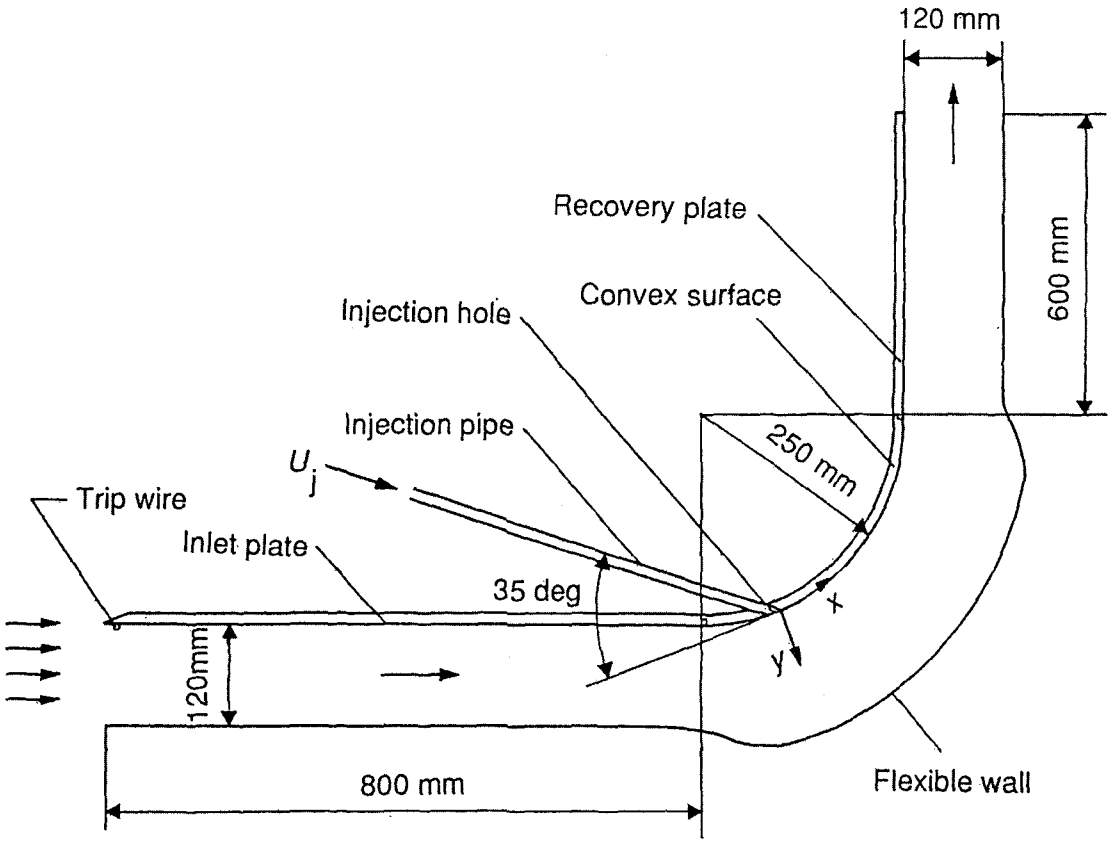

Fig. 1 Schematic of test section

motors (Oriental Motors, PH566-03GK) with linear heads were installed for movements in both y- and z-directions.

In the boundary layer flow, the static pressure at a specific location in the radial direction can be obtained from the inviscid theory when the radius of curvature is given. When there exists a radial pressure gradient on the curved surface, the velocity in the boundary layer may be determined by the following equation (Meroney and Bradshaw, 1975):

$$\frac{U}{U_{pw}}=\left[\left(\frac{P_t-P_r}{P_r-P_{sw}}\right)+e^{-2y/r_w}\right]^{1/2} \tag{1}$$

where P_t is the total pressure, P_r the total pressure outside the boundary layer, P_{sw} the static pressure at the wall, and r_w denotes the radius of curvature. The potential velocity on a curved surface is given by

$$\begin{aligned} U_p &= U_{pw}e^{-y/r_w} \\ &\approx U_{pw}[(1-y/r_w)+O((y/r_w)^2)] \end{aligned} \tag{2}$$

$$U_{pw}=\left[\frac{2}{\rho_\infty}(P_r-P_{sw})\right]^{1/2} \tag{3}$$

Since the potential velocity, U_p, varies linearly in the radial direction, the flow velocity outside the boundary layer is not constant. Hence, in this case, the potential velocity at the wall, U_{pw}, can be adequately used as a reference velocity.

Figure 2 shows the velocity profiles in the symmetry plane of the convex surface. The solid lines denote the potential velocity profiles obtained from Eq. (2). As shown in this figure, the streamwise velocity, U, coincides with the potential velocity, U_p, in the region outside the boundary layer. At the origin of the coordinates, U_{pw} was maintained at 10.5 m/s. At this point the displacement and momentum thicknesses based on potential velocity were 1.86 mm and 1.47 mm,

Table 1 Experimental conditions

	U_{pw} (m/s)	D (mm)	a (deg)	Re_D	ρ_j/ρ_∞	R
Flow visualization	10.5	10	35, 90	0.67×10^4	1.53	0.5, 1.0, 1.5, 2.0
Velocity measurement	10.5	24	35	1.60×10^4	1.00	0.5, 1.98

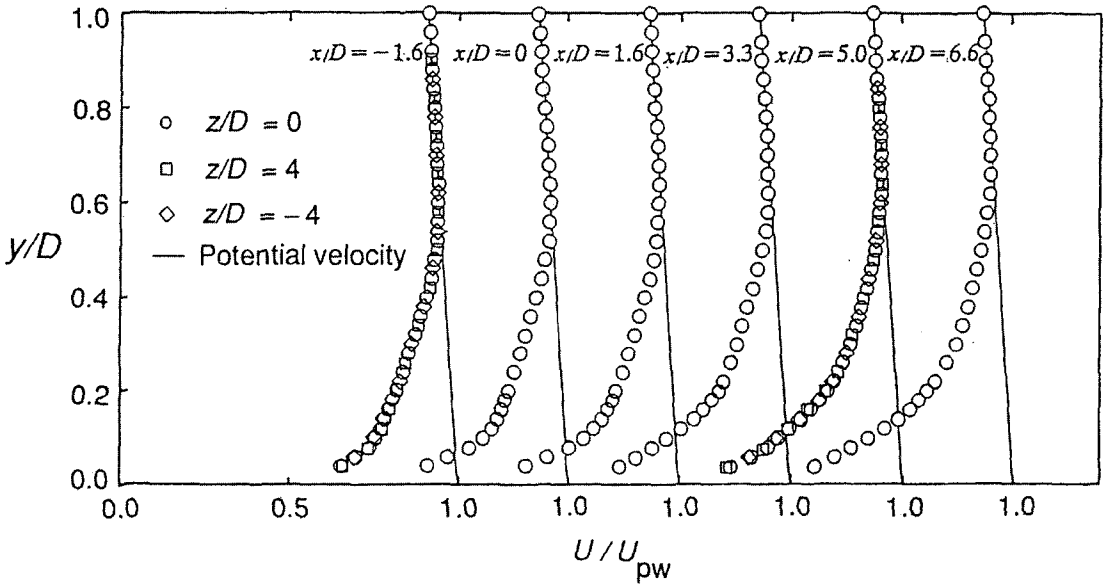

Fig. 2 Boundary layer velocity profiles in the symmetry plane of the convex surface in the absence of injection

respectively. The Reynolds number of the cross-flow at the jet exit was : $Re_{pw}=U_{pw}D/\nu=1.60\times 14^4$. The velocity ratio, U_j/U_{pw} was maintained at 1.98 and the momentum flux ratio, $\rho_j U_j^2/\rho_\infty U_{pw}^2$, was 3.92. At the origin, δ/R which indicated the strength of the curvature, was approximately 0.06 and D/R was 0.096. The measurements were conducted on the six y-z planes, the locations of which were $x/D=-1$, 0, 1, 2, 4 and 6. In each y-z planes, the measuring points were: y/D from 0 to 2.5 and z/D from 0 to 1.5 with an interval of $D/6$ in both directions. The experimental conditions are summarized in Table 1.

Practically the pressure measurement system was the same as that of Lee et al. (1994). The measurement error in the flow angle was estimated within about 1° except near the jet exit where highly turbulent flow was dominant. The error in positioning the probe was estimated at most about 0.2 mm. The accuracy of the measured pressures was within 1% of the dynamic pressure outside the boundary layer. In order to have a precise global estimate of the measurement accuracy, mass flux was evaluated at each boundary surface of measurement arrays. As a result, the net mass flux across all the surfaces of the measurement control volume was balanced to within 2% of total inlet mass flux.

3. Results and Discussion

3.1 Flow visualization

As mentioned above, the injection angle, a, is an important parameter. The injection angle changes the relative magnitude of the centrifugal force acting on a jet fluid element with respect to the force associated with radial injection momentum, which may cause significant changes in the jet trajectory even in the case that the velocity ratios are the same. The effect of the

inclination angle is also going to be discussed in detail later. In the present visualization, the potential velocity at a convex wall is maintained at 10.5 m/s. The density ratio of the jet fluid to mainstream fluid is 1.53, and D/r_w is 0.04.

Figure 3 shows the instantaneous side views of 35° inclined jets injected into the boundary layer on the convex wall with variation of the velocity ratio or momentum flux ratio. When $R=0.5$, the jet is significantly bent toward the wall near the jet exit, and the flow shows very complex turbulent motion. The injected fluid is confined to the restricted region near the wall and the jet trajectory is not separated from the wall even far downstream. On escaping from the hole, the jet is moving toward the wall and fills up the near-wall region downstream. When the velocity ratio is small, the flow downstream of the jet exit is mainly occupied by the jet fluid. This is because the radial pressure gradient and mainstream dynamic pressure play dominant roles. As the velocity ratio reaches 1.5, the jet trajectory is clearly separated from the wall even just downstream of the jet exit, and no jet fluid can be seen near the wall. This implies that there exist strong inward motions of the mainstream fluid toward the jet symmetry plane underneath the jet trajectory, which will be shown clearly later by three-dimensional velocity data. From the convex wall into the radial direction, the downstream turbulent flow field can be divided into three regions ; wake region ; jet region ; and free-stream region. The pressure force by radial static pressure gradient is constant as long as the mainstream conditions are the same, and the force associated with radial injection momentum is also constant independent of radial location if α and R are fixed. However, the centrifugal force acting on an injectant element is proportional to the square of streamwise velocity but inversely proportional to the radial distance from a wall-curvature center. As the velocity ratio increases, the mean radial distance of jet trajectory must become larger, which results in a decrease of the centrifugal force, proportional to square of the streamwise velocity. Therefore, for the 35° injection, the jet trajectory with a large

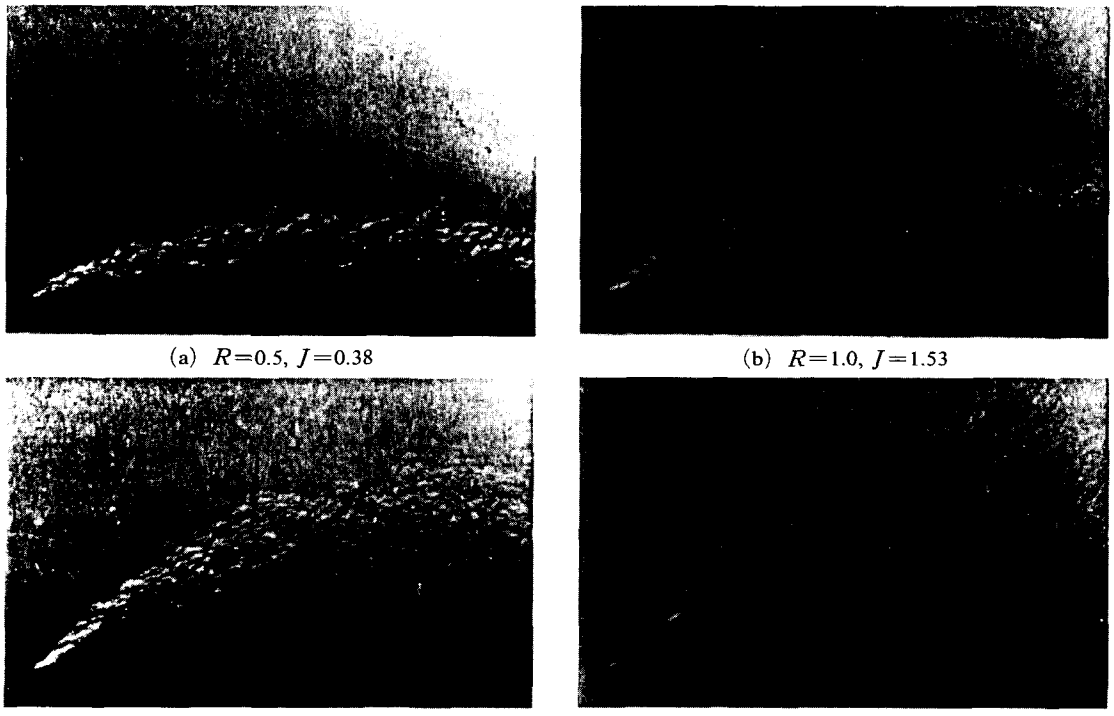

(a) $R=0.5$, $J=0.38$ (b) $R=1.0$, $J=1.53$

(c) $R=1.5$, $J=3.45$ (d) $R=2.0$, $J=6.12$

Fig. 3 Short-exposure Schlieren photographs for 35 deg injection

velocity ratio is departing from the wall in the downstream direction. Though the present jets are injected from a discrete round hole and the resulting flow shows a three-dimensional turbulent nature, the radial force balance based on the two-dimensional flow configuration could still account for the jet behavior adequately from a qualitative view point.

Figure 4 shows the instantaneous flow structure for normal injection. The jet strongly collides with mainstream and widely spreads as the velocity ratio increases. The contribution of the centrifugal force can not be seen, because the jet initially does not have the streamwise velocity component. Near the jet exit, the large normal momentum of the jet interacts with the radial pressure force, and the jet trajectory is bent due to the mainstream dynamic pressure gradient in the streamwise direction. When $R=0.5$, the normally injected jet shows similar trend compared with that of 35° injection. In the case that $R=1.0$, the rolling-up of shear layer is clearly seen just above the jet exit and the lower boundary of the jet always touches the wall surface. For larger velocity ratios such as $R=1.5$ and 2.0, the jet penetrates far into the mainstream, but there still exists the jet fluid touching the convex wall.

In the case of 35° injection, the jet maintains its structure further downstream as on the flat plate (Lee et al., 1994). For a large velocity ratio, the relatively large streamwise momentum causes large centrifugal force, which results in the gradual departure of the jet from the convex wall as moving downstream. On the contrary, for the 90° injection, there is no streamwise momentum, but large normal momentum which causes further penetration of the jet into crossflow. However, the penetration is confined only to the jet exit. In the downstream region, there is no gradual departure of the jet from the wall, since the jet has small streamwise momentum.

3.2 Mean velocity distributions

Since the momentum flux ratio is usually larger than unity in an actual blade cooing system, major emphasis has been placed on the velocity ratio

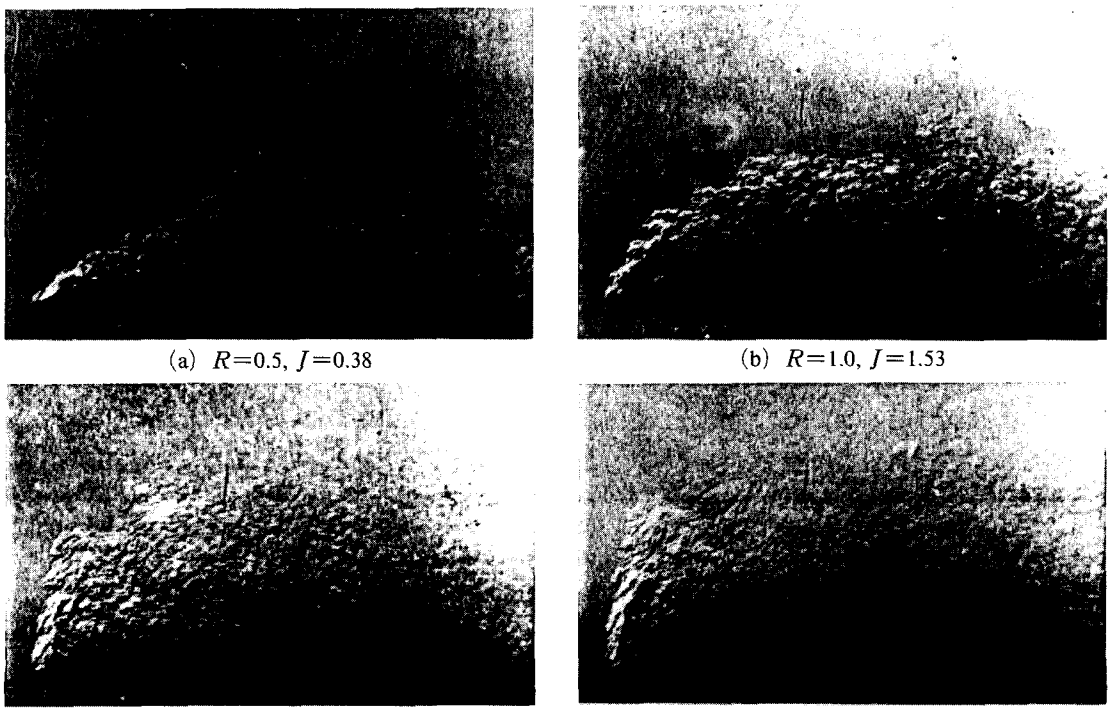

(a) $R=0.5$, $J=0.38$ (b) $R=1.0$, $J=1.53$

(c) $R=1.5$, $J=3.45$ (d) $R=2.0$, $J=6.12$

Fig. 4 Short-exposure Schlieren photographs for 90 deg injection

and the momentum flux ratio of 1.98 and 3.92, respectively. Figure 5 shows the streamwise velocity contours at each measurement plane. As moving downstream, the jet bound or high velocity region is growing and the contours forms a shape like a kidney as in Fig. 5(c). At $x/D=-1$, the region with velocity gradient is confined to near the jet exit and a large velocity gradient

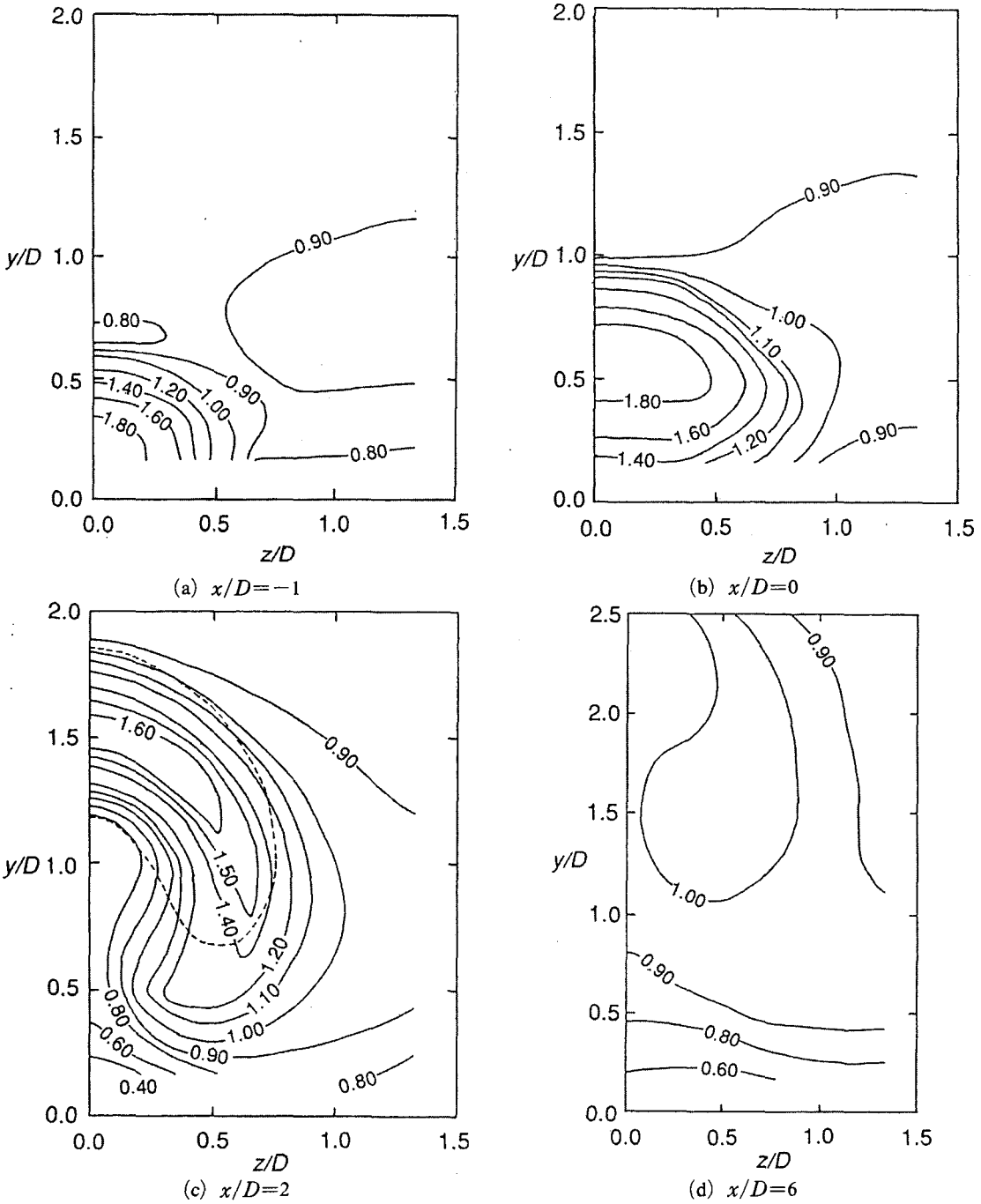

(a) $x/D=-1$ (b) $x/D=0$

(c) $x/D=2$ (d) $x/D=6$

Fig. 5 Contours of streamwise velocity, U/U_{pw}, at $R=1.98$

appears in the vicinity of the interface between the jet and the crossflow, where $y/D=0.5$. Right above the jet, there exists a narrow region where the velocity is decreasing in the y-direction. Streamwise velocity distribution confirms that the jet region extends rapidly especially in the y-direction and the region with larger streamwise velocity is separated from the wall when x/D reaches

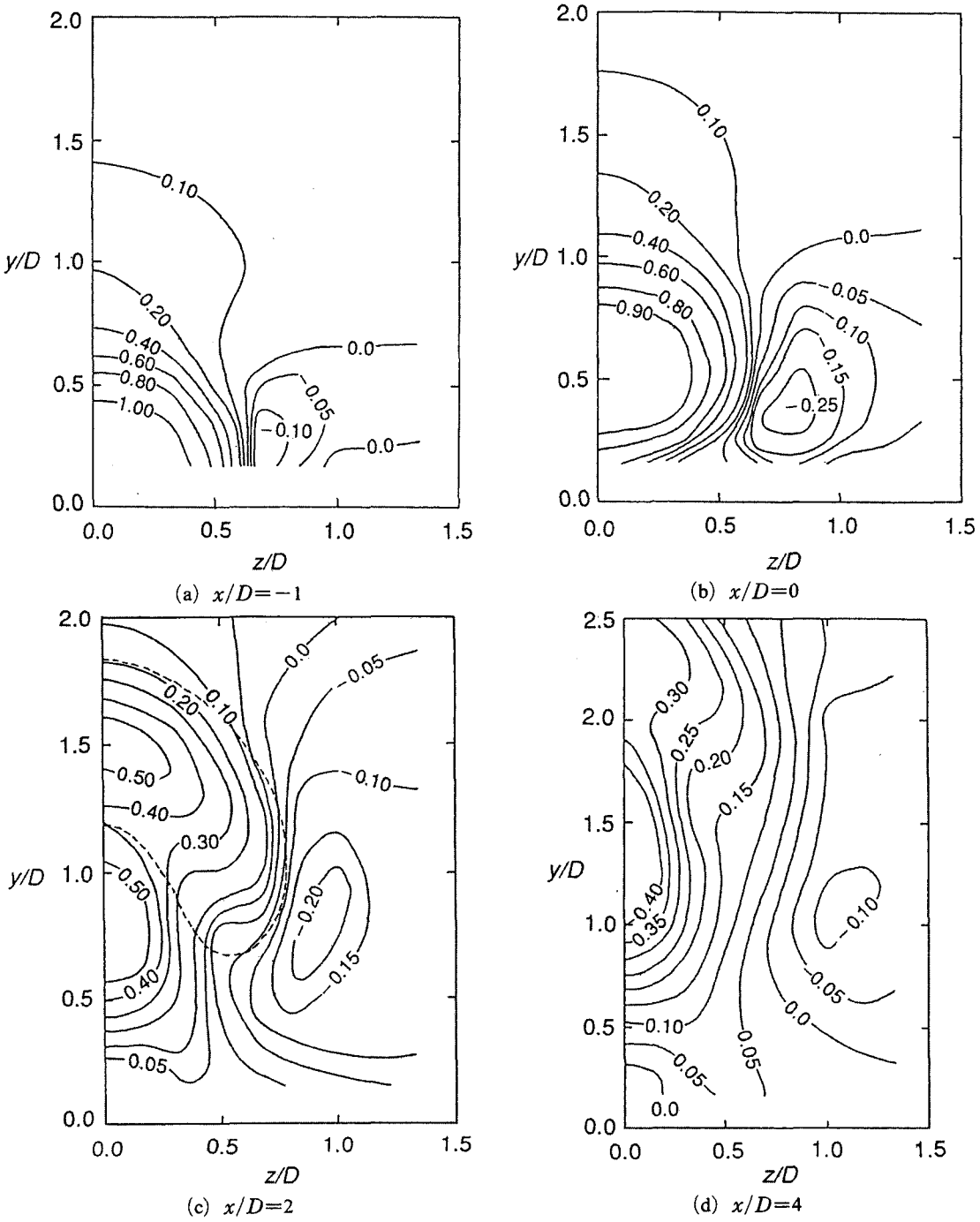

Fig. 6 Contours of radial velocity component, V/U_{pw}, at $R=1.98$

2. At $x/D=2$, the wake region is observed where the streamwise velocity is very small near the jet symmetry plane ($z/D=0$). The wake region is surrounded by the jet region denoted by a dotted line. The dotted line in Fig. 5(c) indicates the interface between the jet and the crossflow determined by the method proposed by Moussa et al. (1977). Due to the departure of the jet from the

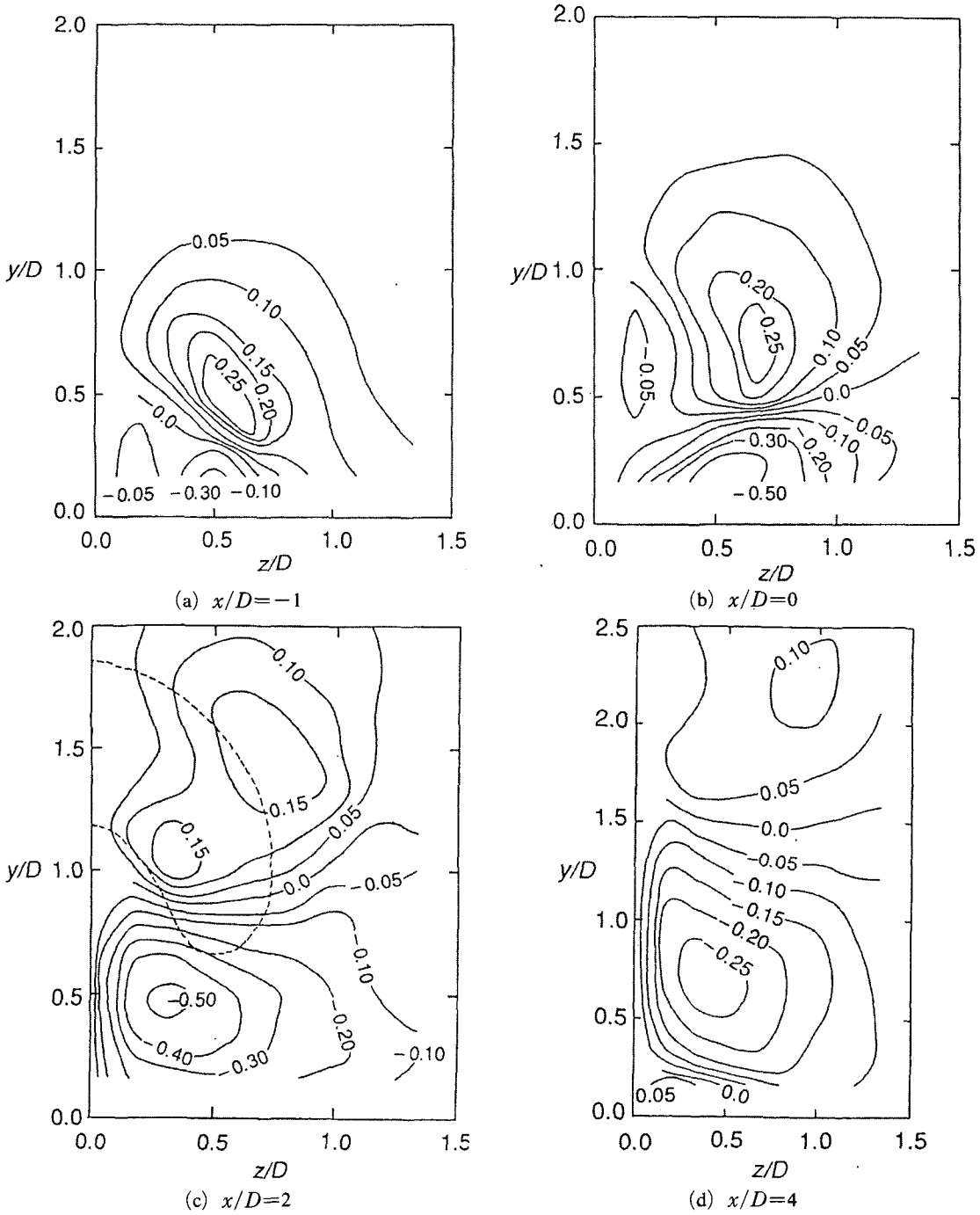

(a) $x/D=-1$ (b) $x/D=0$

(c) $x/D=2$ (d) $x/D=4$

Fig. 7 Contours of spanwise velocity component, W/U_{pw}, at $R=1.98$

wall, the wake region is stretched in the y-direction. Between the flow regions, there are two shear layers where the velocity gradient is relatively large. At $x/D=6$, the jet region spreads far and wide, and accordingly the velocity gradient diminishes and the shear layers become extinct because of shearing and three-dimensional mixing between the jet and the crossflow fluids. However, relatively large velocity gradient appears near the wall, which indicates that the crossflow boundary layer is recovering underneath the jet as the jet effect becomes weakened.

Figure 6 shows a distribution of V/U_{pw} for $R=1.98$. As moving downstream, the region with large radial velocity is extended, and the negative radial velocity region always appears. At $x/D=0$, the maximum radial velocity location is separated from the convex wall, and the maximum value of the negative velocity is the largest in all the measurement planes. At $x/D=-1$ and 0, the jet fluid seems to have the largest radial momentum. At $x/D=2$, two peaks of positive V/U_{pw} are observed in the jet symmetry plane. One is located in the wake region between the jet and the convex wall, and the other in the jet region. At $x/D=4$, it seems that the two peaks merges into one in the wake region. This implies that the radial velocity near the jet exit attributes to the radial component of the jet velocity, but far downstream, it is induced and maintained by inward motion of mainstream fluid into the wake region. As can be seen at $x/D=2$, the magnitude of the radial components described above are comparable with each other.

The spanwise velocity, W/U_{pw}, is shown in Fig. 7. Initially the injected jet has no spanwise momentum, however, due to the interaction with mainstream boundary layer flow, relatively large W has been produced. Near the wall, a strong inward motion is observed regardless of streamwise location, and this region expands in the y-direction downstream. At $x/D=4$, the region with negative W reaches up to $y/D=1.5$.

From three-dimensional mean velocity data for $R=1.98$, it is confirmed that the jet trajectory is separated from the convex wall notably. The flow near the jet exit shows a strong three-dimensional nature with a pair of bound vortices. The large departure of the jet from the convex wall results in expansion of the bound vortex region, and brings about additional vortices near the convex wall at a certain downstream location.

3.3 Mean vorticity distributions

The vortex structure of the jet in a crossflow can be more clearly explained by streamwise vorticity distributions. The streamwise vorticity, Ω_x, can be determined from the circulation in the y-z plane. In Fig. 8, Ω_x has been normalized by the spatially averaged mean vorticity at the injection pipe, Ω_j. Since the direction of the vorticity coming out from the jet pipe is always parallel to the pipe wall, the mean vorticity flux can be defined as in the nomenclature. The calculated values of Φ_j and Ω_j are 14.4 m^3/s^2 and 1744/s, respectively.

Figure 8 shows the dimensionless vorticity, Ω_x/Ω_j, at each y-z plane. In the present coordinate system, the vorticity in the bound vortex region is positive. At $x/D=-1$, Ω_x/Ω_j has its maximum value at $z/D=0.5$. Along the sreamwise direction, the bound vortex region containing positive vorticity, is extended and the location of the maximum positive vorticity coincides approximately with the bound vortex center. The vorticity has its maximum at $x/D=0$, and then decreases gradually in the streamwise direction. As moving downstream, the positive vorticity region is separated from the wall remarkably. At $x/D=2$, a negative vorticity distribution develops into a typical one. At $y/D=1.5$, near the jet symmetry plane, nearly zero vorticity region is found, which is equivalent to a potential core region or inside of the jet boundary. This typical vorticity distribution is sustained further downstream even at $x/D=6$, though its strength is weakened significantly as it diffuses away. Just below the bound vortex being separated from the wall, a negative vortex region is somewhat expanding near the wall, which is attributed to the counter rotating vortex. At $x/D=6$, the absolute values of both positive and negative vorticities are nearly the same. The jet boundary is determined by using the mean vorticity as in Moussa et al. (1977). Figure 8(c) shows how the jet boundary

is determined from the vorticity distributions. The dotted line, which is defined as jet-crossflow interface, always passes the ridges of vorticity contours.

3.4 Effect of velocity ratio

As shown in the jet trajectory, the wall curvature influences the jet behavior differently depending on the velocity ratio. Here, the velocity

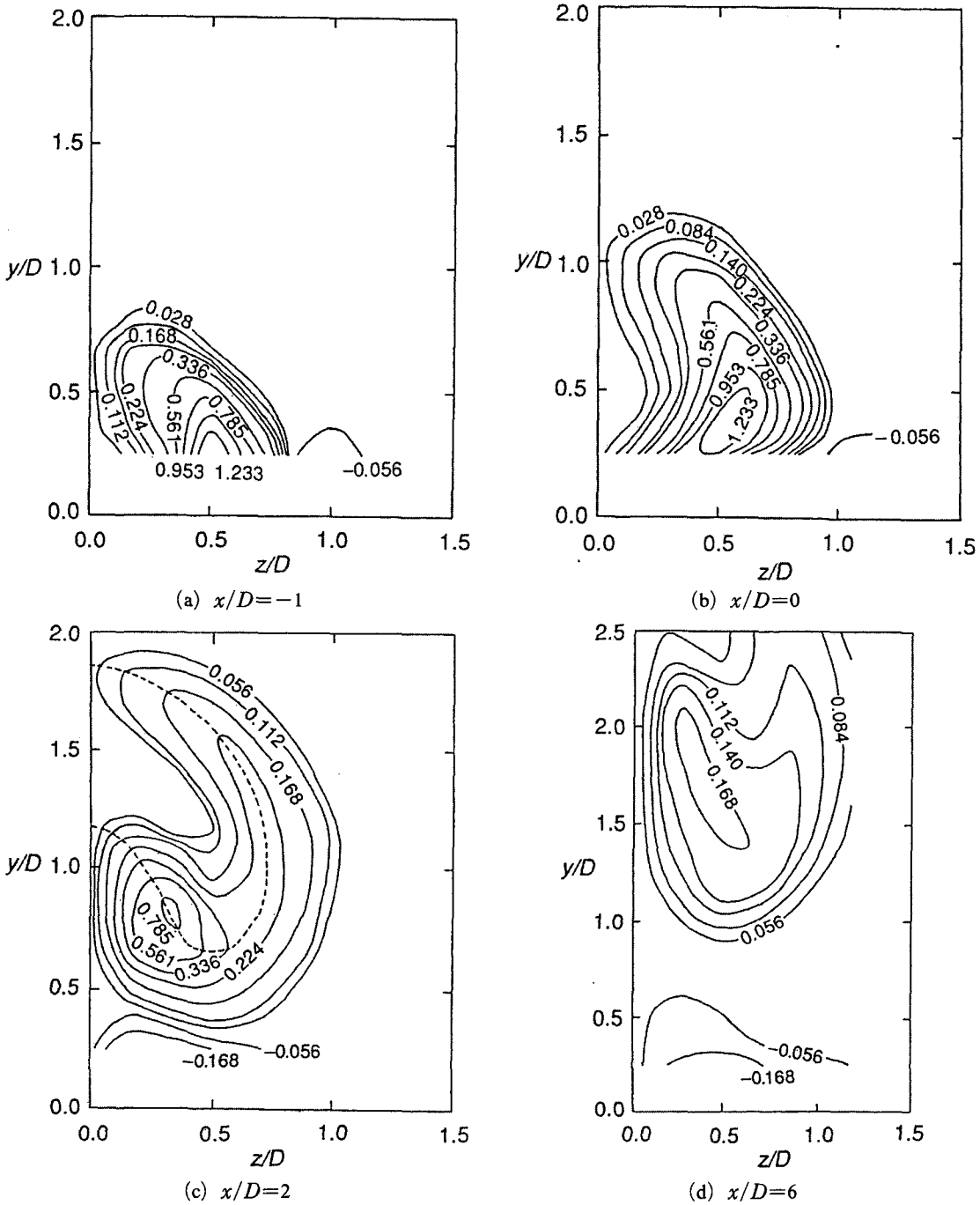

Fig. 8 Contours of streamwise vorticity component, Ω_x/Ω_j, at $R=1.98$

profiles in the jet symmetry plane for $R=1.98$ are compared with those for $R=0.5$. In this case, the momentum flux ratio, J, is 0.25. Figure 9 compares the x-directional velocity profiles. Generally, on the convex surface, the potential velocity is decreasing, departing from the convex wall. The solid straight lines in Fig. 9 represent potential velocity profile obtained from Eq. (2). The result shows that there is a good agreement between the potential velocity from Eq. (2) and the x-directional velocity measured by using the five-hole pressure probe beyond the boundary layer or in the region where the jet effect is negligible. When $R=0.5$, the jet does not influence significantly the boundary layer flow except for the near-wall region. In comparison of the x-directional velocity near the wall along the streamwise direction, it shows a maximum at $x/D=0$ because of acceleration of the jet fluid caused by shearing with the crossflow, on the other hand, it is the smallest at $x/D=1$ because of the presence of wake. In the downstream region, the momentum diffusion and shearing between the jet and the crossflow results in the increase in the x-

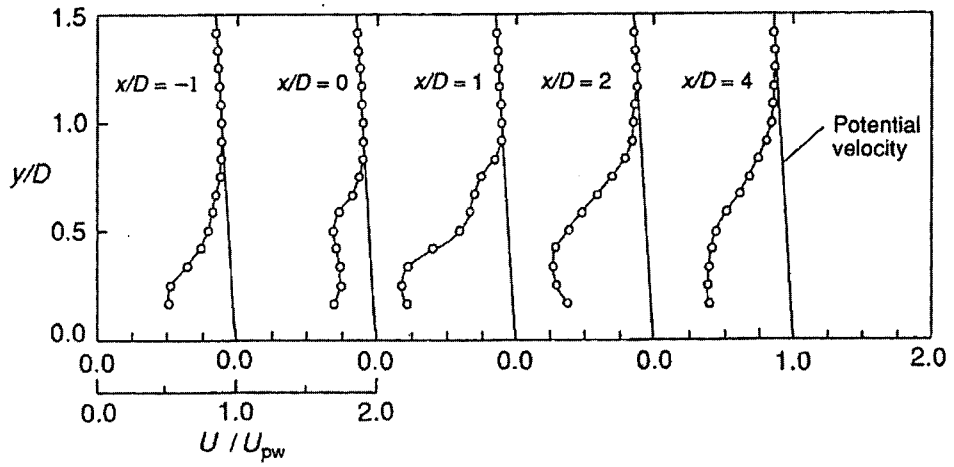

(a) $R=0.5$

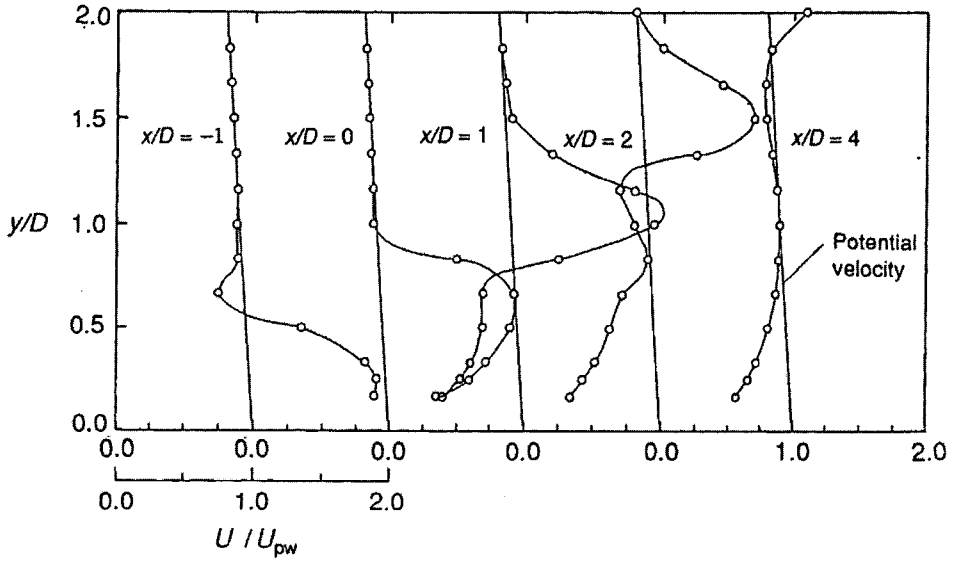

(b) $R=1.98$

Fig. 9 Streamwise velocity profile in the jet symmetry plane

directional velocity near the wall and the expansion of jet area in the radial direction. In the case of $R=1.98$, the velocity profile appears totally different from that for $R=0.5$. The jet region grows drastically and the higher velocity region is clearly separated from the wall. At $x/D=-1$, the velocity value is less than unity near $y/D=0.7$ because of deceleration of the crossflow as approaching the jet. At $x/D=2$, another peak in the streamwise velocity profile near $y/D=0.8$ is observed, but the peak value does not exceed the potential velocity at the wall. This means the mainstream boundary layer is redeveloping near the wall.

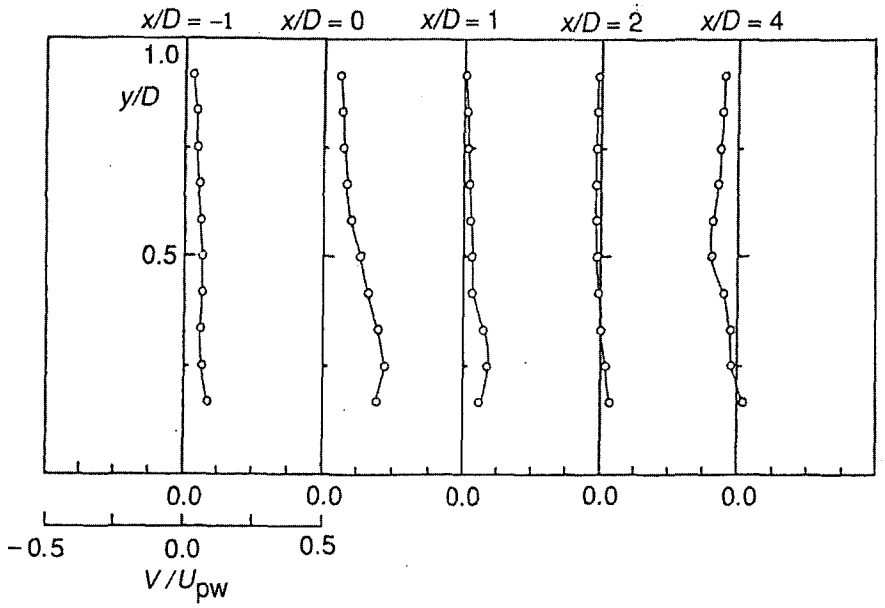

(a) $R=0.5$

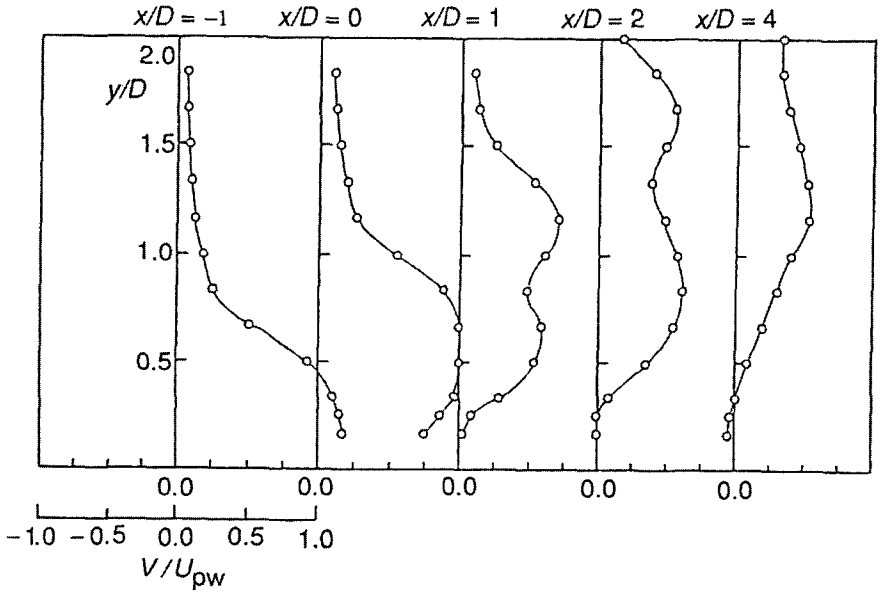

(b) $R=1.98$

Fig. 10 Radial velocity profile in the jet symmetry plane

In Fig. 10, y-directional velocity profiles in the jet symmetry plane are presented. When $R=0.5$, V/U_{pw} near the convex wall has positive value due to the y-component of injection velocity. However, the y-directional velocity magnitude is decreasing as moving downstream. Arriving at $x/D=2$, there exists a flow moving toward the wall except for the near-wall region, which becomes much stronger at $x/D=4$. This means that at $x/D=2$, the bound vortex structure, which is dominant in the case of $R=1.98$, is no longer existent for $R=0.5$. In addition, for a small velocity ratio such as $R=0.5$, the pressure gradient in the crossflow forces the jet fluid to move toward the convex wall, stabilizing and reducing the secondary motion. This kind of flow phenomenon is also observed by Ko et al. (1984). On the contrary, in the case of $R=1.98$, the region with larger velocity is rapidly growing just after the jet exit and is expanded in the y-direction. At $x/D=1$, there are two peaks of V/U_{pw} in the y-direction. One of them is located in the wake region and the other one in the jet region. The peak near the wall has slightly smaller value than the other peak. This indicates that in the region near the jet exit, the jet fluid coming out of the injection pipe has larger y-directional momentum than the mainstream fluid induced in the wake. On the other hand, when x/D is larger than 2, the mainstream fluid in the wake has larger y-directional momentum than the jet fluid. Accordingly, in the relatively far downstream region, the upward motion departing from the convex wall is due mainly to the pressure drop in the wake resulting from the large separation of the jet trajectory from the wall, not to the y-directional momentum of the jet. This was also observed on a flat plate (Lee, 1994). At $x/D=4$, a flow moving toward the convex wall can be seen near the wall, which results from the counter-rotating vortex opposite to the bound vortex near the wall.

In the case of a small velocity ratio, the radial pressure gradient causes the downwash of the jet which causes the jet fluid to move toward the wall, and the convex curvature stabilizes the jet flow. As a result, the bound vortex structure has been destroyed. However, for a large velocity ratio, the increases in both y-directional momentum and the centrifugal force from the x-directional momentum result in wider separation of the injected jet from the wall. Due to separation, a very strong bound vortex appears and its structure tends to persist far downstream. This separation also produces another counter-rotating vortices near the wall.

4. Conclusions

The effect of convex curvature on film cooling jet behavior has been investigated. Three-dimensional velocity components were measured in the near field of the jet exit and in the downstream region for a 35° inclined injection. The global flow behaviors of 35° and 90° injections were compared through flow visualization study. Some important observations are noticed and summarized below.

(1) From visualization, it is confirmed that the jet trajectory depends strongly on the centrifugal force, which makes the jet separated from the wall gradually for a large velocity ratio. Meanwhile, at 90° injection, it seems that the jet is not affected by the centrifugal force any more and its path near the jet exit is characterized by the strong normal momentum. In the case of a small velocity ratio, jets of both 35°and 90° injections show similar trend.

(2) An attempt to explain the curvature effect on the jet flow through radial force balance has been made. The flow visualization results for both 35° and 90° jets can be interpreted by a simple force balance consideration, which provides some insight in understanding the curvature effect, and the role of streamwise injection momentum has been emphasized.

(3) With the three-dimensional mean velocity data of R=1.98, it is confirmed that the jet trajectory is separated from the convex wall significantly, however, the near-field of jet flow shows very strong three-dimensional flow with a pair of bound vortices. The increases in both y-directional momentum and the centrifugal force from x-directional momentum overcome the radial pressure gradient. Due to separation, a pair

of strong bound vortices emerges and its structure tends to persist far downstream. This separation also produces another counter-rotating vortices with respect to the bound vortex downstream near the convex wall. In the case of a small velocity ratio $R=0.5$, the radial pressure gradient causes downwash of the jet moving toward the wall, and the convex curvature stabilizes the jet flow. As a result, the bound vortex structure has been destroyed.

Acknowledgment

This work was supported in part by the Micro Thermal System Research Center through the Korea Science and Engineering Foundation.

References

Andreopoulos, J., 1985, "On the Structure of Jets in a Crossflow," *J. Fluid Mechanics*, Vol. 157, pp. 163~197.

Andrepoulos, J, and Rodi, W., 1984, "Experimental Investigation of Jets in a Crossflow," *J. Fluid Mechanics*, Vol. 138, pp. 93~127.

Kamotani, Y. and Greber, I., 1972, "Experiment on a Turbulent Jet in a Cross Flow." *AIAA J.*, Vol. 10, pp. 1425~1429.

Keffer, J. F. and Baines, W. D., 1963, "The Round Turbulent Jet in a Cross-wind," *J. Fluid Mechanics*, Vol. 15, pp. 481~496.

Ko, S. Y., Xu, J. Z., Yao, Y. O. and Tsou, F. K., 1984, "Film Cooling Effectiveness and Turbulence Distribution of Discrete Holes on a Convex Surface," *Int. J. Heat Mass Transfer*, Vol. 27, pp. 1551~1557.

Lee, S. W., Lee, J. S. and Ro, S. T., 1994, "Experiment Study on the Flow Characteristics of Streamwise Inclined Jets in Crossflow on Flat Plate," *ASME J. Turbomachinery*, Vol. 116, pp. 97~105.

Meroney, R. N. and Bradshaw, P., 1975, "Turbulent Boundary-Layer Growth over a Longitudinally Curved Surface," *AIAA J.*, Vol. 13, pp. 1448~1453.

Morton, B. R., 1961, "On a Momentum-mass Flux Diagram for Turbulent Jets, Plumes and Wakes," *J. Fluid Mechanics*, Vol. 10, pp. 101~108.

Moussa, Z. M., Trischka, J. W. and Eskinazi, S., 1977, "The Near-Field in the Mixing of a Round Jet with a Cross-stream," *J. Fluid Mechanics*, Vol. 80, pp. 49~80.